

Brown adipose tissue lipoprotein and glucose disposal is not determined by thermogenesis in uncoupling protein 1-deficient mice

Alexander W. Fischer¹, Janina Behrens, Frederike Sass, Christian Schlein, Markus Heine, Paul Pertzborn, Ludger Scheja, and Joerg Heeren*¹

Department of Biochemistry and Molecular Cell Biology, University Medical Center Hamburg-Eppendorf, Hamburg, Germany

Abstract Adaptive thermogenesis is highly dependent on uncoupling protein 1 (UCP1), a protein expressed by thermogenic adipocytes present in brown adipose tissue (BAT) and white adipose tissue (WAT). Thermogenic capacity of human and mouse BAT can be measured by positron emission tomography-computed tomography quantifying the uptake of ¹⁸F-fluodeoxyglucose or lipid tracers. BAT activation is typically studied in response to cold exposure or treatment with β -3-adrenergic receptor agonists such as CL316,243 (CL). Currently, it is unknown whether cold-stimulated uptake of glucose or lipid tracers is a good surrogate marker of UCP1-mediated thermogenesis. In metabolic studies using radiolabeled tracers, we found that glucose uptake is increased in mildly cold-activated BAT of *Ucp1*^{-/-} versus WT mice kept at subthermoneutral temperature. Conversely, lower glucose disposal was detected after full thermogenic activation achieved by sustained cold exposure or CL treatment. In contrast, uptake of lipoprotein-derived fatty acids into chronically activated thermogenic adipose tissues was substantially increased in UCP1-deficient mice. This effect is linked to higher sympathetic tone in adipose tissues of *Ucp1*^{-/-} mice, as indicated by elevated levels of thermogenic genes in BAT and WAT. Thus, glucose and lipoprotein handling does not necessarily reflect UCP1-dependent thermogenic activity, but especially lipid uptake rather mirrors sympathetic activation of adipose tissues.

Supplementary key words adipocytes • lipase/lipoprotein • lipid metabolism • lipase/hormone-sensitive • lipid transport • lipolysis and fatty acid metabolism • lipoprotein metabolism • triglycerides

Brown adipose tissue (BAT) is a heat-producing organ in mammals and important for physiological adaptation to cold environments (1). Its thermogenic function is regu-

lated by the sympathetic nervous system in response to low ambient temperature. BAT activity and mass in relation to body mass are exceptionally high in small mammals (1) as well as in newborn humans (2, 3) but were, until recently, believed to be negligible in adults. However, some years ago, studies measuring glucose uptake by positron emission tomography-computer tomography (PET-CT), a technique commonly used for identification of tumor metastases, detected BAT as distinct regions of high glucose uptake in adult humans exposed to cold temperatures (4–8). Histological and expression analysis confirmed that these foci indeed represent BAT (9, 10).

Due to its high oxidative capacity, activated BAT has profound metabolic effects and can reduce blood triglycerides (11) and cholesterol (12) as well as glucose levels (13). In the context of cardiometabolic diseases, BAT activation favorably affects atherosclerosis (12), lipoprotein remodeling (14), and cholesterol metabolism (15) in mice. In humans it has been shown that cold exposure decreases body weight (16, 17), and several PET-CT studies reported an inverse relationship between detectable BAT volume and incidence of obesity/type 2 diabetes (4, 5, 17–23). Thus, BAT mass, as measured by uptake of labeled glucose in PET-CT, is predictive of metabolic health in humans. However, this method may not be a reliable measure for BAT function, as lipoprotein-derived triglyceride but not glucose is the main fuel for BAT thermogenesis (11, 24), and thus lipid uptake may be a better predictor. Even more importantly, energy uptake into BAT may not be directly linked to BAT oxidative thermogenic capacity in a close mechanistic fashion (25). One experimental model to address the question of whether lipid uptake into BAT correlates with its thermogenic capacity is mice lacking uncoupling protein 1 (UCP1). This mitochondrial proton transporter enables thermogenesis in brown adipocytes by uncoupling respiration from ATP production (1). While *Ucp1*^{-/-} mice are surprisingly resistant to obesity when housed under standard housing conditions of mild cold exposure (26), they develop aggravated obesity when housed under warm thermoneutral temperatures (27, 28). Thermoneutrality is defined as the temperature range where no extra energy expenditure is needed for maintaining

This article contains [supplemental data](#).

*For correspondence: Joerg Heeren, heeren@uke.de

Present address of Alexander W. Fischer: Department of Molecular Metabolism, Harvard T. H. Chan School of Public Health, Boston, MA and Department of Cell Biology, Harvard Medical School, Boston, MA.

Present address of Frederike Sass: Novo Nordisk Foundation Center for Basic Metabolic Research, University of Copenhagen, Copenhagen, Denmark.

Present address of Christian Schlein: Institute of Human Genetics, University Medical Center Hamburg-Eppendorf, Hamburg, Germany.



body temperature and is the typical living condition for humans (29–31).

In the present study, we set out to quantify glucose and lipid fluxes in *Ucp1*^{-/-} mice housed under conditions of minimal BAT activity (thermoneutrality, 30°C), mild BAT activity (standard housing conditions, 22°C), and maximum BAT activity (cold exposure at 6°C or pharmacological BAT activation). Uptake of both lipids and glucose was lower in UCPI-deficient mice in response to acute pharmacological BAT stimulation. In contrast, we observed that UCPI deficiency is not associated with reduced glucose and lipid uptake under thermoneutral and standard conditions, but that *Ucp1*^{-/-} mice rather display increased clearance of these energy substrates. Under conditions of chronic maximal BAT activation, however, *Ucp1*^{-/-} mice display a peculiar switch in nutrient preference as shown by reduced glucose uptake and a concomitantly increased lipid uptake into BAT. These data indicate that neither glucose nor lipid uptake can be used as a direct measure of UCPI-dependent BAT thermogenic capacity under homeostatic conditions.

MATERIALS AND METHODS

Mice and experimental conditions

All mouse experiments were approved by the Animal Welfare Officers of University Medical Center Hamburg-Eppendorf and Behörde für Gesundheit und Verbraucherschutz Hamburg. *Ucp1*^{-/-} mice [B6.129-*Ucp1*^{tm1Kz}/J, Jackson Laboratory stock 003124 (26)] were kindly provided by Jan Nedergaard and Barbara Cannon, Stockholm University, and at the animal facility of University Medical Center Hamburg-Eppendorf backcrossed with C57BL6/J mice. Heterozygous mice were bred to generate WT and *Ucp1*^{-/-} mice. Note that in supplemental Fig. S4 and Fig. 4I–P, heterozygous mice were used as controls. The mice were kept at a 12/12 h light/dark cycle and had ad libitum access to drinking water and regular chow diet (P1324, Altromin, Germany). Male or female age-matched mice (12–16 weeks old) were used as indicated in the figure legends.

Fat tolerance test

Mice were housed at 22°C or 30°C for 7 days. After a 4 h daytime fast, each mouse received a lipid gavage with 200 mg triolein, 20 mg lecithin, and 3.5 mg cholesterol emulsified in 250 µl NaCl. Blood samples were taken by tail vein puncture before and 60, 120, and 240 min after gavage. Mice were anesthetized with ketamine (180 mg/kg body weight) and xylazine (24 mg/kg body weight) before BAT samples were harvested for histological analysis and measurement of tissue lipid and protein content.

Oral glucose fat tolerance with radioactive tracers

For an oral glucose and fat tolerance test (OGFT), mice were fasted for 4 h before receiving an oral gavage of 300 µl of a glucose-lipid emulsion containing 47 mg/kg body weight triglycerides from Intralipid® and 2 g/kg body weight glucose, traced with ³H-deoxyglucose (³H-DOG) (0.72 MBq/kg body weight) and ¹⁴C-triolein (0.15 MBq/kg body weight). For oral glucose tolerance tests, the gavage contained 2 g/kg body weight glucose, traced with ¹⁴C-deoxyglucose (0.15 MBq/kg body weight). Two hours after gavage, anesthetized mice were transcardially perfused with PBS containing 10 U/ml heparin to release lipoproteins attached

to endothelial walls. Organs were harvested, weighed, and dissolved in 10× (v/w) Solvable™ (Perkin Elmer), and radioactivity (in disintegrations per minute) was measured by scintillation counting using a Perkin Elmer Tricarb scintillation counter.

Clearance of radiolabeled triglyceride-rich lipoproteins

The preparation of radioactively labeled triglyceride-rich lipoproteins (TRLs) was performed as described previously (32). Briefly, chloroform extracts from TRLs isolated from hypertriglyceridemic human plasma were traced with ¹⁴C-triolein and ³H-cholesterylhexadecylether (both purchased from Perkin Elmer). Then, solvents were evaporated, and the lipids were suspended in 0.9% NaCl by sonication and filtered through 0.45 µm filter as described (32). For simultaneously measuring the clearance of injected TRLs and glucose, TRLs were prepared with ¹⁴C-triolein, and the injection solution was spiked with ³H-DOG (0.72 MBq/kg body weight). Mice were fasted for 4 h before intravenous injection with 200 µl of the radiolabeled TRL solution (triglycerides: 80 mg/kg) double-labeled with ³H-cholesterylhexadecylether (2.5 MBq/kg) and ¹⁴C-triolein (0.6 MBq/kg) (32). Mice were anesthetized 20 min after injection, transcardially perfused with PBS containing 10 U/ml heparin, and organs were harvested for scintillation counting as described above.

Western blotting and antibodies

Western blotting was performed using standard procedures (33, 34). Briefly BAT samples were homogenized in 10× (v/w) RIPA buffer [50 mM Tris-HCl (pH 7.4), 5 mM EDTA, 150 mM sodium chloride, 1 mM sodium pyrophosphate, 1 mM sodium fluoride, 1 mM sodium orthovanadate, 1% NP-40] supplemented with cOmplete™ Mini Protease Inhibitor Cocktail tablets (Roche) in a tissue lyser (Qiagen). Lysates were centrifuged at 16,000 g for 10 min, the clear soluble middle layer without the fat cake was taken, and protein concentration was determined using a BCA kit (Thermo). Twenty micrograms of total protein in NuPAGE reducing sample buffer (Invitrogen) were denatured at 60°C for 10 min and separated on 10% SDS-polyacrylamide Tris-glycine gels. Transfer to nitrocellulose membranes was performed in a wet blotting system; membranes were stained with Ponceau S (Serva) to confirm equal loading, washed twice in TBS-T [20 mM Tris, 150 mM sodium chloride, 0.1% (v/v) Tween 20] and blocked in 5% milk powder (Sigma) in TBS-T for 1 h at room temperature. Primary antibody incubation (5% BSA in TBS-T) was performed overnight at 4°C. Secondary antibodies were diluted in 5% milk powder in TBS-T, and detection was performed with enhanced chemiluminescence using an Amersham Imager 600 (GE Healthcare).

The following primary antibodies were used: rabbit-anti-acetyl-CoA carboxylase (ACC; 1:1,000; Cell Signaling #3662), rabbit-anti-cluster of differentiation 36 (CD36) (1:5,000; provided by Kathryn Moore; New York), rabbit-anti-cAMP response element-binding protein (CREB; Cell Signaling #9197), rabbit-anti-phospho-CREB (Ser133; Cell Signaling #9198), rabbit-anti-deiodinase type 2 (DIO2; 1:1,000; Abcam ab77779), mouse-anti-FASN (1:500; BD Bioscience #610962), rabbit-anti-glucose transporter 4 (GLUT4; 1:1,000; provided by Anette Schürmann, Potsdam, Germany), rabbit-anti-hormone-sensitive lipase (HSL; Cell Signaling #4107), rabbit-anti-phospho-HSL (Ser563; Cell Signaling #4139), chicken-anti-LPL (1:2,000; provided by Stefan Nilsson, Umeå, Sweden), rabbit-anti-tyrosine hydroxylase (TH; 1:5,000; Abcam ab137869), rabbit-anti-γ-tubulin (g-TUB; 1:2,500; Abcam ab179503), rabbit-anti-UCP1 (1:25,000; provided by Jan Nedergaard, Stockholm, Sweden). All of the following secondary HRP-coupled antibodies were from Jackson ImmunoResearch and diluted 1:5,000: rabbit-anti-chicken HRP (#303-035-003), goat anti-mouse HRP (#115-035-003), goat-anti-rabbit HRP (#111-035-144, WB 1:5000).

Gene expression analysis

Total RNA was isolated using NucleoSpin RNA II kit (Macherey and Nagel). After synthesis of cDNA, quantitative real-time PCR was performed and the relative expression of genes of interest was calculated by normalization to housekeeper TATA-box binding protein (*Tbp*) as described (15). The following TaqMan Assay-on-Demand primer sets (Applied Biosystems) were used: acetyl-CoA carboxylase 1 (*Acaca*), Mm01304285_m1; angiopoietin-like 4 (*Angptl4*), Mm00480431_m1; *Cd36*, Mm00432403_m1; *Dio2*, Mm00515664_m1; elongation of very long chain fatty acids 3 (*Elovl3*), Mm00468164_m1; *Fasn*, Mm00662319_m1; *Glut4*, Mm01245502_m1; *Lpl*, Mm00434764_m1; *Tbp*, Mm00446973_m1; *Ucp1*, Mm00494069_m1.

BAT triglyceride content and histology

For measurement of BAT triglyceride content, lysates were prepared in 10× (v/w) RIPA buffer as described above and centrifuged at 2,000 *g* for 10 min at 4°C. Supernatants including the fat cake were harvested and triglyceride concentration was determined using a commercial colorimetric kit (Roche). Afterwards, the lysate was centrifuged for an additional 10 min at 16,000 *g* and the soluble middle layer was taken for measurement of protein content using a BCA kit (Thermo).

For histology, adipose tissues were fixed in 3.6% formalin in phosphate-buffered saline. H&E staining was performed on sections of paraffin-embedded tissues using standard procedures (35). Images were taken using a NikonA1 Ti microscope equipped with a DS-Fi-U3 brightfield camera. Quantification of adipocyte number and size in H&E stainings was performed using the Adiposoft plugin for Fiji/ImageJ (36).

Statistics

Data are expressed as mean ± SEM. Student's *t*-test or two-way ANOVA were used for comparison between groups. Microsoft Excel 2016 and GraphPad Prism 6.0 were used for statistical calculations. *P* < 0.05 was considered to be statistically significant. Only significant differences between genotypes are shown.

RESULTS

UCP1 deficiency increases clearance of both lipid and glucose into mildly activated BAT

To determine how the lack of thermogenic capacity in BAT of *Ucp1*^{-/-} mice impacts on systemic lipid handling, we performed an oral fat tolerance test in WT and *Ucp1*^{-/-} mice. The animals were acclimated to standard housing conditions (22°C) that confer mild BAT activation, or to thermoneutral conditions (30°C) where BAT displays negligible thermogenic activity. In comparison to WT mice, we observed lower plasma triglycerides in response to the fat gavage in *Ucp1*^{-/-} mice housed at 22°C (Fig. 1A). In contrast, no differences were observed in mice housed under thermoneutral conditions (Fig. 1B). Histological analysis revealed a higher number and enlarged size of lipid droplets in BAT of *Ucp1*^{-/-} versus WT mice at 22°C (Fig. 1C), which was also reflected by a higher BAT weight (supplemental Fig. S1A) and triglyceride content (supplemental Fig. S1B). These genotype-dependent differences were less pronounced when mice were housed at thermoneutrality (Fig. 1D; supplemental Fig. S1A, B). BAT weight was only increased by trend in thermoneutral BAT of *Ucp1*^{-/-} mice

in this cohort (supplemental Fig. S1A); yet in a separate experiment (supplemental Fig. S5B), we did observe significantly increased BAT weight at thermoneutrality, principally in agreement with (27). The increased lipid droplet size and BAT triglyceride content in *Ucp1*^{-/-} mice have been noted previously (26, 37, 38) and are believed to be a reflection of reduced triglyceride oxidation. However, the lower triglyceride levels after the fat tolerance test (Fig. 1A) are suggestive for higher disposal of TRLs into BAT of *Ucp1*^{-/-} mice, which could additionally contribute to the expanded BAT lipid stores in *Ucp1*^{-/-} mice. To address this hypothesis, we performed a metabolic turnover study using recombinant TRLs labeled with ¹⁴C-triolein and non-metabolizable ³H-cholesterylether (³H-CE), the latter as a label for the lipoprotein core. After intravenous injection of radiolabeled TRLs into mice housed at 22°C, we found higher specific (Fig. 1E) and total (Fig. 1F) uptake of radiolabeled triolein into BAT of *Ucp1*^{-/-} versus WT mice. A similar but less pronounced effect was observed for the radioactive lipoprotein core label (Fig. 1G, H). The uptake into other tissues was not affected by the genotype (supplemental Fig. S1C, D).

To investigate the metabolic clearance of dietary glucose and lipids in a physiological postprandial setting, we performed an OGFT with the radiolabeled tracers ³H-DOG and ¹⁴C-triolein in WT and *Ucp1*^{-/-} mice acclimated to 22°C or thermoneutral conditions. In line with the increased TRL clearance in *Ucp1*^{-/-} mice housed at 22°C (Fig. 1E–H), we observed higher specific (Fig. 1I) and total triglyceride (Fig. 1J) uptake into BAT of *Ucp1*^{-/-} versus WT mice. The effect was less pronounced and not significant under thermoneutral conditions (Fig. 1I, J). It is of note that *Ucp1*^{-/-} mice housed at 22°C also displayed higher uptake of ³H-DOG into BAT (Fig. 1K, L). As shown in supplemental Fig. S1E and F, the disposal of triglycerides or glucose was not affected by the genotype in any other organs investigated. Fasting glucose, triglycerides, and cholesterol as well as FFAs were not affected by genotype, while *Ucp1*^{-/-} mice acclimated to thermoneutral conditions displayed elevated insulin levels (supplemental Fig. S2A–E). Taken together, despite a lack of nonshivering thermogenesis, mildly activated BAT of *Ucp1*^{-/-} mice unexpectedly exhibited a higher uptake of glucose and lipids than BAT of WT mice.

Thermogenic markers are increased in BAT and WAT of *Ucp1*^{-/-} mice

The activity of BAT nutrient uptake and thermogenic activity is controlled by the sympathetic nervous system (1). To examine the activity of the sympathetic pathway, we analyzed the expression of thermogenic marker genes in BAT of WT and *Ucp1*^{-/-} mice housed at 22°C or thermoneutrality (Fig. 2A). As expected, subthermoneutral housing resulted in higher expression of the thermogenic markers *Dio2* and *Elovl3*. This effect was even more pronounced in *Ucp1*^{-/-} mice, suggesting a higher sympathetic tone in BAT in the absence of UCPI. In agreement with previous findings (39, 40) and as indicated by higher gene expression of thermogenic markers in this tissue (supplemental Fig. S2F),

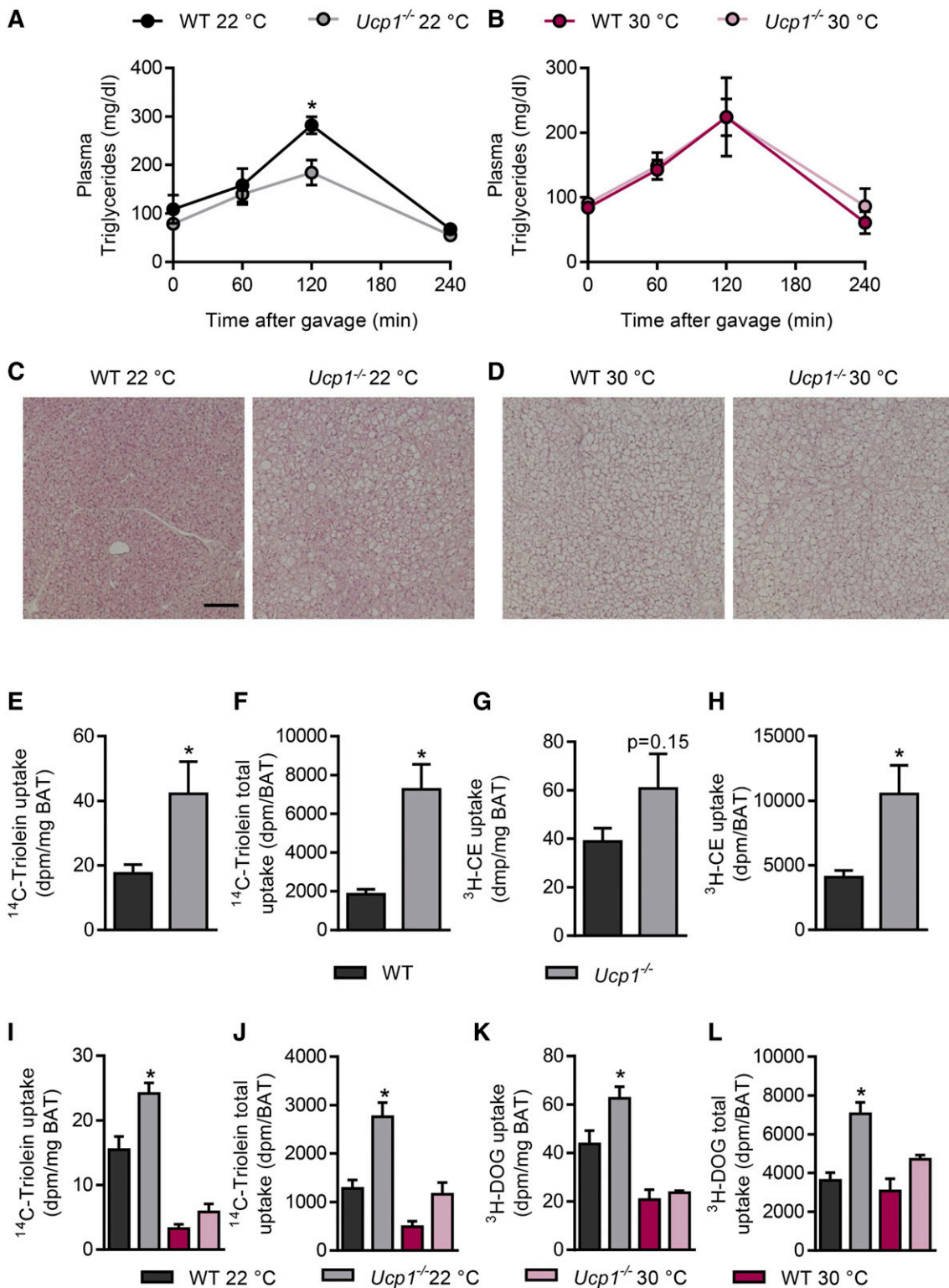


Fig. 1. Increased clearance of lipid and glucose by BAT in *Ucp1*^{-/-} mice housed below thermoneutrality. Male WT and *Ucp1*^{-/-} mice were acclimated to 22°C or 30°C and plasma lipid clearance as well as BAT morphology and nutrient uptake were measured. A, B: Plasma triglyceride levels following oral lipid gavage in WT and *Ucp1*^{-/-} mice at 22°C (A) and 30°C (B) (n = 4–5). C, D: H&E staining of BAT sections from the mice described in A and B (scale bar: 100 μm). E–H: Uptake of recombinant TRLs labeled with ³H-cholesterylether (³H-CE) and ¹⁴C-triolein in mice housed at 22°C (n = 7–8). Specific (E) and total organ (F) ¹⁴C-triolein uptake into interscapular BAT (iBAT). Specific (G) and total organ (H) ³H-CE uptake into iBAT. I–L: Oral combined glucose and fat tolerance test traced with ¹⁴C-triolein and ³H-DOG in WT and *Ucp1*^{-/-} mice housed at 22°C or 30°C (n = 5–6). Specific (I) and total (J) ¹⁴C-triolein uptake into iBAT. Specific (K) and total (L) ³H-DOG uptake into iBAT. *P < 0.05 by Student's *t*-test or two-way ANOVA. Only significant differences between genotypes in the same interventional group are indicated.

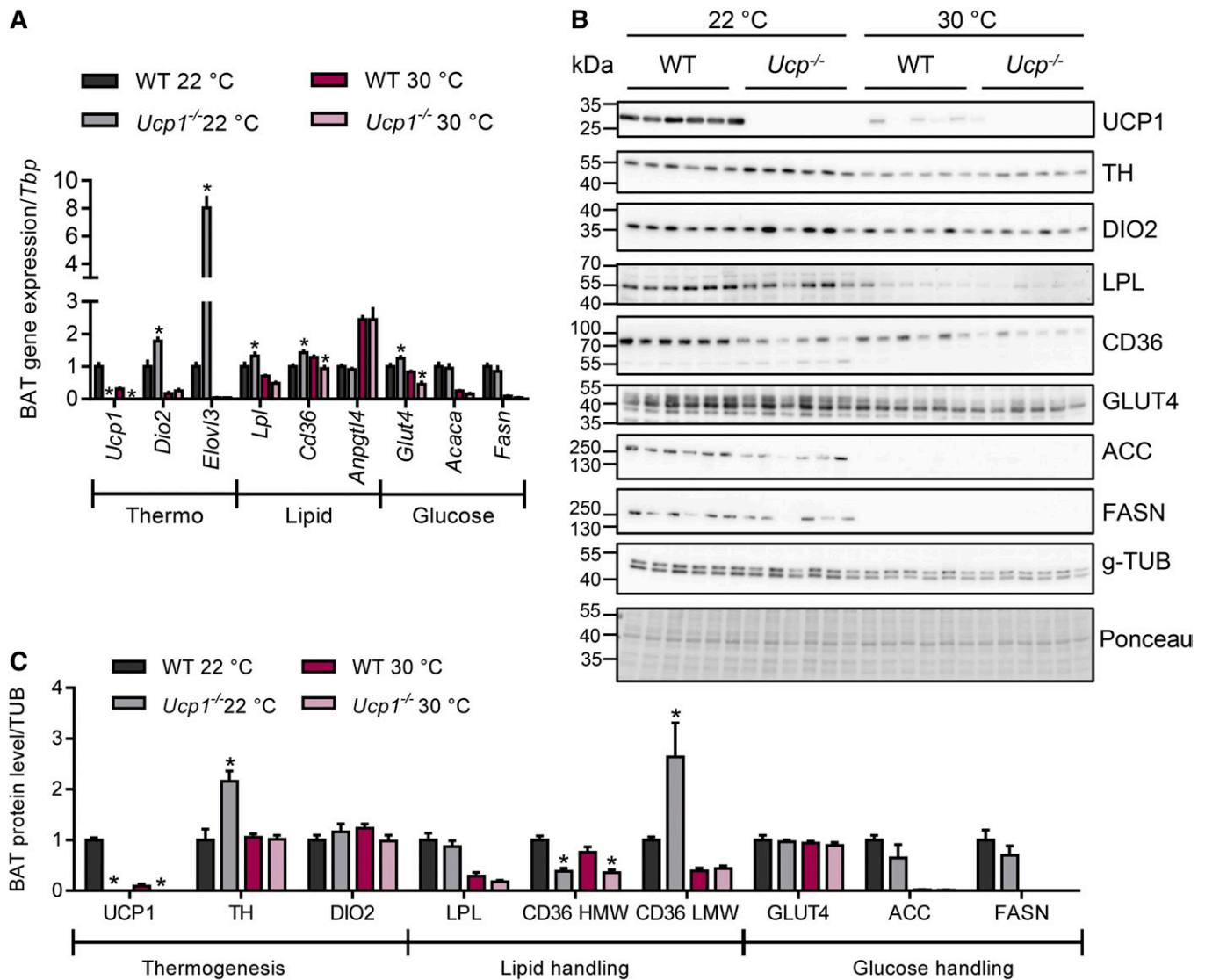


Fig. 2. Expression of thermogenic and nutrient handling genes in iBAT of WT and *Ucp1*^{-/-} mice. BAT samples from male WT and *Ucp1*^{-/-} mice acclimated to 22°C or 30°C were harvested for mRNA and protein analyses (n = 5–6). A: mRNA expression of indicated genes in iBAT, values are shown relative to WT 22°C. B: iBAT Western blot analysis using specific antibodies to indicated proteins. C: Quantification of Western blots, values were normalized to the housekeeper g-TUB and shown relative to WT 22°C. **P* < 0.05 by two-way ANOVA. Only significant differences between genotypes in the same interventional group are depicted. HMW, high-molecular-weight; LMW, low-molecular-weight.

sympathetic tone appeared to also be increased in inguinal white adipose tissue (iWAT) of knockout mice housed under subthermoneutral conditions. To more directly assess sympathetic activity in UCP1-deficient BAT, we measured the phosphorylation of protein kinase A (PKA) target proteins including CREB and HSL in BAT of WT and *Ucp1*^{-/-} mice acclimated to 22°C. In line with the hypothesis that sympathetic tone was elevated in *Ucp1*^{-/-} mice, phosphorylation of CREB and HSL as well as the abundance of TH were higher in UCP1-deficient mice than in WT controls (supplemental Fig. S2G, H).

Next, to investigate the molecular basis for the observed increased nutrient uptake into *Ucp1*^{-/-} BAT at 22°C, we measured expression of genes involved in lipid uptake (*Lpl*, *Cd36*, *Angptl4*), as well as in glucose uptake and metabolism (*Glut4*, *Acaca*, *Fasn*) in BAT of mice acclimated to

22°C or 30°C (Fig. 2A). As recently shown (41, 42), most of these metabolic genes showed a strong regulation by the ambient temperature with de novo lipogenesis-related genes, *Acaca* and *Fasn*, being most strongly downregulated at thermoneutrality, whereas gene expression of the LPL-inhibitor, *Angptl4*, was upregulated in inactive BAT (Fig. 2A). In line with increased glucose and lipid uptake (Fig. 1), an upregulation of *Lpl*, *Cd36*, and the glucose transporter *Glut4* was observed in BAT of *Ucp1*^{-/-} compared with WT mice housed at 22°C (Fig. 2A). In iWAT, the expression of lipid and glucose handling genes was mostly unaltered (supplemental Fig. S2F), which is consistent with similar nutrient uptake into iWAT of WT and UCP1-deficient mice (supplemental Fig. S1E, F).

To validate the observations made in BAT on the protein level, we analyzed the expression of thermogenic markers

(UCP1, DIO2), as well as players of lipid metabolism (LPL, CD36) and glucose metabolism (GLUT4, ACC, FASN) in BAT samples from the mice described above by Western blotting (Fig. 2B, C). The majority of the proteins analyzed exhibited a profound regulation by housing temperature, while genotype had no significant effect on the abundance of most proteins. However, and in further support of an increased sympathetic tone in the absence of UCP1, we found elevated protein expression of TH, the rate-limiting enzyme of norepinephrine synthesis, in BAT of *Ucp1*^{-/-} versus WT mice housed at 22°C (Fig. 2B, C). Notably, the levels of the inactive high-molecular-weight CD36 were specifically reduced in *Ucp1*^{-/-} mice, while the low-molecular-weight isoform, which is thought to represent the active form (32, 43), was specifically increased in BAT of *Ucp1*^{-/-} mice housed at subthermoneutral conditions. Lower expression of the housekeeper tubulin in the samples from thermoneutrally housed mice may compromise the comparison between samples from mice housed at different temperatures; however, equal protein loading was shown by Ponceau staining. Taken together, these findings indicate that UCP1 deficiency leads to altered sympathetic tone at subthermoneutral temperatures, which in turn may drive the increased nutrient uptake into BAT.

UCP1 deficiency alters energy disposal in thermogenic adipose tissues of cold-acclimated mice

UCP1-deficient mice are acutely sensitive to cold exposure but can be gradually acclimated to colder temperatures (37, 44–47). Several alternative heat-producing mechanisms have been proposed to be functional in *Ucp1*^{-/-} mice that could mediate the cold tolerance following gradual acclimation, including thermogenesis in WAT and BAT (48–51) as well as muscle (45, 52).

To investigate the role of UCP1-dependent thermogenesis for nutrient handling under conditions of maximal BAT activation and WAT browning, we performed an OGFT in cold-acclimated *Ucp1*^{-/-} versus WT mice. While specific lipid uptake into BAT was comparable between genotypes (Fig. 3A), total organ uptake was doubled in *Ucp1*^{-/-} mice (Fig. 3B). Notably, specific glucose uptake was decreased by 50% in BAT of *Ucp1*^{-/-} compared with WT mice (Fig. 3C), whereas total BAT uptake was similar (Fig. 3D). The differences between specific and total uptake of both lipid and glucose can be explained by the higher BAT weight of cold-acclimated *Ucp1*^{-/-} mice (supplemental Fig. S3A). These results are reflected by comparable fasting glucose levels (supplemental Fig. S3B), while fasting triglyceride and cholesterol levels were decreased in cold-acclimated *Ucp1*^{-/-} mice (supplemental Fig. S3C, D), which is in line with previous observations (39). Plasma FFA and insulin levels were also comparable between genotypes (supplemental Fig. S3E, F).

To understand the molecular basis of the alterations in glucose and lipid uptake into BAT of cold-acclimated *Ucp1*^{-/-} mice, we analyzed the levels of genes and proteins involved in adaptive thermogenesis as well as glucose and lipid metabolism in BAT of WT and *Ucp1*^{-/-} mice. Gene expression of thermogenic markers *Dio2* and *Elavl3* was induced in

UCP1-deficient BAT (Fig. 3E), and so were protein levels of TH and DIO2 (Fig. 3F, G), both pointing toward increased sympathetic tone even at 6°C. In line with increased lipid uptake, the transcript levels of *Lpl* and *Cd36* were increased in BAT of *Ucp1*^{-/-} mice (Fig. 3E), and, interestingly, *Angptl4* expression was also increased, possibly being part of a negative feedback loop to limit lipid uptake as described before (42). LPL protein levels, as well as the levels of the active low-molecular-weight form of CD36 were increased in UCP1-deficient BAT (Fig. 3F, G). Consistent with decreased glucose uptake, mRNA and protein levels of ACC and FASN were strongly reduced in *Ucp1*^{-/-} BAT (Fig. 3F, G). Notably, some variability in housekeeper levels was observed, which did not affect the interpretation of the data, however, and was not due to unequal protein loading.

Next to adaptive recruitment of BAT, sustained cold exposure leads to the browning of various WAT depots, a process characterized by the appearance of thermogenic UCP1-positive brite/beige adipocytes (53–55). To investigate the consequences of UCP1 deficiency for energy handling by brite/beige adipocytes, we determined lipid and glucose uptake in iWAT of cold-acclimated *Ucp1*^{-/-} versus WT mice. Notably, we found an approximately 4-fold increase in the specific and total organ uptake of ¹⁴C-triolein (Fig. 3H, supplemental Fig. S3G). In contrast to BAT, ³H-DOG uptake was also slightly but significantly increased in iWAT (Fig. 3I, supplemental Fig. S3H). Increased gene expression of the thermogenic markers *Dio2* and *Elavl3* indicated a more pronounced browning in iWAT of *Ucp1*^{-/-} mice (Fig. 3J). This is presumably caused by a higher sympathetic activity in this tissue that, together with higher *Lpl* expression (Fig. 3J), can explain the substantially increased lipid uptake. In contrast to BAT, expression of *Glut4*, *Fasn*, and *Acaca* was higher in iWAT of cold-acclimated *Ucp1*^{-/-} mice (Fig. 3J), which is consistent with increased ³H-DOG uptake (Fig. 3I). The abovementioned experiments were performed in female mice. However, all major findings were essentially reproduced in male *Ucp1*^{-/-} mice, including alterations in organ weights (supplemental Fig. S4A) and plasma lipid levels (supplemental Fig. S4B, C), switch in fuel preference (supplemental Fig. S4D–G) as well as signs of increased sympathetic tone in both BAT (supplemental Fig. S4J–L) and iWAT (supplemental Fig. S4M). Overall, these data demonstrate that energy uptake into BAT and iWAT of cold-acclimated mice is independent of UCP1-mediated thermogenesis. Moreover, the already very high lipid uptake into both BAT and iWAT of cold-acclimated mice is further induced in the absence of UCP1, which may be explained by a compensatory increase in sympathetic tone in thermogenic adipose tissues of *Ucp1*^{-/-} mice. The decreased glucose uptake with accompanying increases in lipid uptake (Fig. 3A–D) could be explained by substrate competition due to the Randle cycle (56). To examine whether this was the case, we performed a glucose-only gavage and determined the uptake of radiolabeled glucose into metabolically active organs of cold-acclimated WT and *Ucp1*^{-/-} mice in the absence of simultaneous supply of dietary lipids (supplemental Fig. S3I–L). Notably, we again observed a

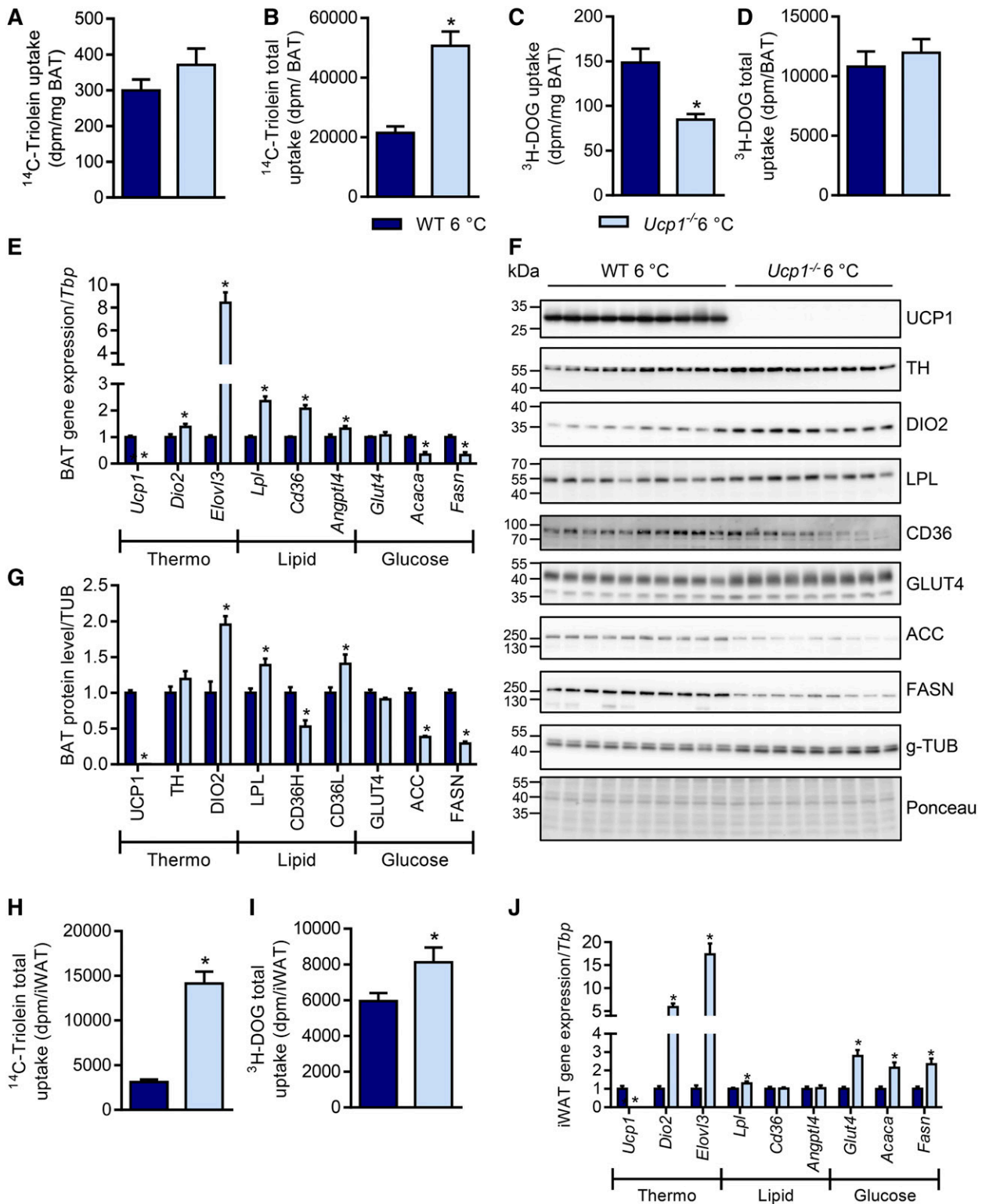


Fig. 3. UCP1 deficiency alters energy disposal in thermogenic adipose tissues of cold-acclimated mice. Female WT and *Ucp1*^{-/-} mice were gradually acclimated to 6°C and gene expression as well as nutrient uptake were measured. For this purpose, mice were kept for 1 week at 18°C and then acclimated to 6°C for 3 weeks before being subjected to an OGFT (n = 8–10). Specific (A) and total (B) ^{14}C -triolein uptake into iBAT. Specific (C) and total (D) ^3H -DOG uptake into iBAT. Expression of mRNA (E) shown relative to WT and protein (F) by Western blot of iBAT samples. G: Quantification of Western blots, values were normalized to g-TUB and shown relative to WT. Total iWAT uptake of ^{14}C -triolein (H) and ^3H -DOG (I). J: iWAT gene expression normalized to *Tbp*, values are shown relative to WT. **P* < 0.05 by Student's *t*-test.

pronounced decrease in BAT glucose uptake into BAT of cold-acclimated *Ucp1*^{-/-} mice as compared with WT mice (supplemental Fig. S3I, J). Interestingly, uptake into iWAT

and muscles increased (supplemental Fig. S3K, L). These data further indicate that the decreased glucose uptake into UCP1-deficient BAT upon strong thermogenic activation

is an intrinsic characteristic of the tissue and not secondary to increased lipid uptake.

UCP1 deficiency differentially modulates lipid and glucose uptake into thermogenic adipose tissues after sustained β -3-adrenergic receptor stimulation

The observed strong induction of nutrient uptake into the BAT of *Ucp1*^{-/-} mice at subthermoneutral temperatures as well as the reductions in glucose uptake in the BAT of cold-acclimated *Ucp1*^{-/-} mice caused us to wonder whether these were secondary effects due to sympathetic overstimulation of the tissue or whether they were a direct consequence of UCP1 deficiency. To address this question, we induced thermogenesis and browning by chronic treatment of WT and *Ucp1*^{-/-} mice housed at thermoneutrality with the β -3-adrenergic receptor agonist CL316,243 (CL) for 1 week. Under this condition, the strength of adrenergic signaling should be comparable between WT and *Ucp1*^{-/-} mice, and direct effects of UCP1 deficiency should be come visible. CL treatment resulted in no alterations in body weight (supplemental Fig. S5A). Compared with control mice housed at thermoneutrality, the injection of CL caused reductions in the weights of thermogenic adipose tissues (supplemental Fig. S5B), which can be explained by lipid combustion and WAT browning. The reduction in iWAT weight was significantly smaller in *Ucp1*^{-/-} mice, indicating that proper UCP1-dependent thermogenesis was at least partially required for the reductions in WAT mass upon CL treatment (supplemental Fig. S5B). BAT lipid uptake was strongly induced by CL treatment in WT mice, and even more pronounced in *Ucp1*^{-/-} mice (Fig. 4A, B). Interestingly, this genotype effect was absent in iWAT and other organs (Fig. 4C, D; supplemental Fig. S5C). Plasma lipid values were reduced by CL treatment but comparable in WT and *Ucp1*^{-/-} mice (supplemental Fig. S5D, E). Remarkably, agonism of β -3-adrenergic receptors by CL strongly induced glucose uptake into BAT of WT mice, and this effect was markedly diminished in *Ucp1*^{-/-} mice (Fig. 4E, F), reminiscent of the effects observed in cold-exposed mice shown in Fig. 3C. In iWAT, the CL and genotype effects were similar but less prominent (Fig. 4G, H), and in other organs they were absent (supplemental Fig. S5G). Notably, the lower glucose uptake into thermogenic adipose tissues of *Ucp1*^{-/-} mice compared with WT mice in response to CL treatment was paralleled by higher plasma glucose levels (supplemental Fig. S5F). The lipolytic effect of CL was not affected by the absence of UCP1, as histological analysis revealed similar decreases in lipid content reflected by adipocyte size in BAT and epididymal WAT (eWAT) of WT and *Ucp1*^{-/-} mice treated with CL (supplemental Fig. S5H, I). Similarly, tissue weights of BAT and eWAT were equally decreased in WT and *Ucp1*^{-/-} mice treated with CL (supplemental Fig. S5B). In summary, a higher lipid uptake into BAT of *Ucp1*^{-/-} mice was observed under conditions of chronic stimulation with the β -3-adrenergic receptor agonist CL. Interestingly, the opposite effect was found for glucose disposal in mice lacking UCP1.

Previous studies examining glucose uptake into UCP1-deficient BAT employed short-term activation protocols

combined with either measurement of glucose by PET-CT (57) or scintillation counting (58). To examine the effects of UCP1 deficiency on lipid uptake under such conditions, we treated room temperature-acclimated mice with CL for 4 h at thermoneutrality and followed the clearance of injected ¹⁴C-triolein-labeled TRLs and a tracer dose of ³H-DOG (Fig. 4I–P). CL treatment induced both lipid and glucose uptake into BAT of WT mice (Fig. 4I, J, M, N), while this response was severely blunted in *Ucp1*^{-/-} mice. Uptake into iWAT (Fig. 4K, L, O, P) as well as uptake into other metabolic organs was largely unaffected (supplemental Fig. S6B, C) and so were organ weights, with the exception of higher BAT weight in *Ucp1*^{-/-} mice (supplemental Fig. S6A). These findings of reduction of both lipid and glucose uptake were strikingly different from the fuel switch observed upon long-term activation (Figs. 3, 4; supplemental Fig. S4). Plasma analysis revealed increased triglyceride levels in CL-treated *Ucp1*^{-/-} mice (supplemental Fig. S6D), while cholesterol and glucose levels were unaffected (supplemental Fig. S6E, F). The acute effect of CL treatment on BAT nutrient uptake is largely dependent upon insulin signaling (24). The effect of CL treatment on insulin signaling is mediated by lipolysis-driven FFA release from WAT that then triggers pancreatic insulin secretion. Interestingly, both FFA levels and plasma insulin levels (supplemental Fig. S6G, H) were more than doubled in acutely CL-treated *Ucp1*^{-/-} mice as compared with WT controls. Taken together, these findings indicate that, in contrast to chronic activation, acute pharmacological BAT stimulation results in lower lipid uptake in *Ucp1*^{-/-} mice, which may be explained by high plasma FFA levels and/or impaired insulin signaling in BAT of UCP1-deficient mice.

DISCUSSION

UCP1 is a protein expressed exclusively by brown and brite/beige adipocytes that mediates efficient heat production in response to increased sympathetic tone in a process known as adaptive nonshivering thermogenesis (1). To sustain high energy expenditure, BAT and brite/beige WAT internalize high amounts of nutrients, in particular TRL-derived fatty acids (11, 12, 24), albumin-bound fatty acids (24, 32, 59, 60), and glucose (24, 34, 61, 62). Especially, the uptake of the glucose tracer ¹⁸F-fluodeoxyglucose has been utilized to determine volume and activity of BAT in humans (4–6, 8, 63, 64). Fatty acid tracers have also been used to detect active BAT (65, 66), whereas TRL tracers for PET-CT studies are under development but need to be improved for human studies (67). Although it is of high relevance for the interpretation of PET-CT studies, it is unclear whether nutrient uptake is directly connected to the dominant thermogenic process mediated by UCP1 (25). In the present study, we addressed this question by comparing glucose and lipid uptake using radiolabeled tracers in WT versus *Ucp1*^{-/-} mice under distinct thermogenic conditions. Recent PET-CT studies using an acute activation protocol of nonshivering thermogenesis by injection of β -adrenergic agonists in *Ucp1*^{-/-} mice concluded that BAT glucose

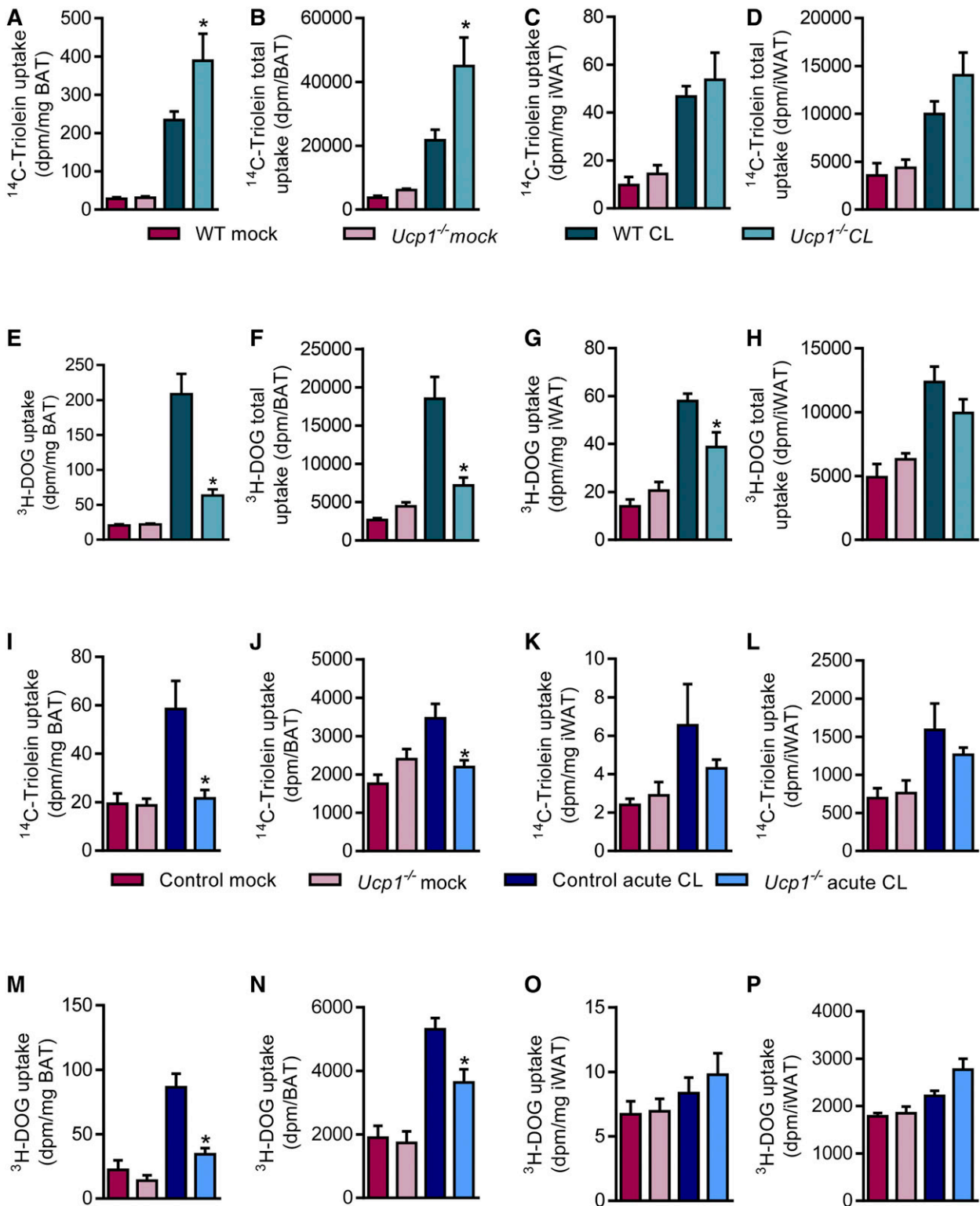


Fig. 4. Nutrient uptake after sustained and acute pharmacological activation with β -3-adrenergic receptor agonism into thermogenic adipose tissues of WT and *Ucp1^{-/-}* mice. For sustained activation, male WT and *Ucp1^{-/-}* mice were housed at 30°C for 1 week and injected daily with 1 mg/kg CL or vehicle (0.9% saline) intraperitoneally before an OGFT was performed (n = 6–8). Specific (A) and total (B) uptake of ¹⁴C-triolein into iBAT. Specific (C) and total (D) uptake of ¹⁴C-triolein into iWAT. Specific (E) and total (F) uptake of ³H-DOG into iBAT. Specific (G) and total (H) uptake of ³H-DOG into iWAT. For acute activation, male control and *Ucp1^{-/-}* mice were housed at 30°C for 1 day and injected with 1 mg/kg CL or vehicle. Four hours after CL injection, ¹⁴C-triolein-labeled TRLs and a tracer dose of ³H-DOG were administered (n = 5–6). Specific (I) and total (J) uptake of ¹⁴C-triolein into iBAT. Specific (K) and total (L) uptake of ¹⁴C-triolein into iWAT. Specific (M) and total (N) uptake of ³H-DOG into iBAT. Specific (O) and total (P) uptake of ³H-DOG into iWAT. **P* < 0.05 by two-way ANOVA. Only significant differences between genotypes in the same interventional group are depicted.

uptake was independent of UCP1 (57, 68). Such studies generally employ intravenous or intraperitoneal injection of radioactive tracers, which is different from the physiological postprandial situation where additional pathways such as insulin secretion, incretin signaling, and a more gradual increase in the plasma levels of glucose and lipids can be observed. Using a postprandial test as a setting more closely resembling this physiological situation, we here show impaired glucose disposal under sustained thermogenic stimulation using cold exposure as well as CL injection in *Ucp1*^{-/-} mice. This is principally in agreement with an earlier study showing lack of induction of glucose uptake into BAT of acutely cold-exposed male *Ucp1*^{-/-} mice (69). Notably, lipid uptake was substantially higher in cold-exposed and CL-treated *Ucp1*^{-/-} mice. While cold exposure induces norepinephrine secretion that triggers the activation of several classes of adrenergic receptors, the pharmacological approach here will only trigger activation of β 3-adrenergic receptors. However, the close resemblance of the phenotypes observed under cold and chronic CL conditions imply that a large proportion of the cold-induced phenotype can indeed be mimicked by β 3-adrenergic activation. Our findings demonstrate a direct link between glucose and UCP1-dependent adaptive thermogenesis, whereas an inverse association was found for TRL-derived lipids.

It has been shown that adrenergic signaling increases glucose uptake into brown adipocytes in a process that is dependent on mTOR complex 2 and GLUT1 (70). Moreover, in immortalized brown adipocytes, thermogenesis was dependent on functional glycolysis and glucose uptake (71), while the absolute contribution of glucose to the energy uptake into BAT is only modest (25, 62, 72). The role of glucose metabolism in BAT thermogenesis may therefore rather lie in providing glycerol for fatty acid reesterification or substrates for de novo lipogenesis (41, 73, 74). Here, we show that sympathetic tone in adipose tissues of *Ucp1*^{-/-} mice is higher when mice are exposed to mild or severe cold (Figs. 2, 3), which could explain the higher glucose uptake into BAT of UCP1-deficient mice acclimated to mild cold (Fig. 1). On the other hand, under conditions of sustained cold exposure or especially after acute or prolonged β -3-adrenergic receptor agonism, glucose uptake into BAT was lower in the knockout mice (Figs. 3, 4). BAT glucose uptake has previously been found to be unaltered in *Ucp1*^{-/-} mice upon acute activation (57, 68), while others found it to be impaired in UCP1 deficiency (58, 69). This discrepancy may be explained by use of anesthesia or the previous housing temperature of the mice. Moreover, it has been shown that glucose uptake into BAT is also driven by insulin-dependent signaling processes (63). In addition to its direct action on brown adipocytes, CL treatment provokes profound fatty acid release by WAT that in turn stimulates insulin secretion by pancreatic β cells (75). Along this line, we showed that glucose uptake into BAT in response to CL treatment is mainly driven by insulin signaling and is impaired in insulin-resistant mouse models (24). It is known that BAT of cold-exposed *Ucp1*^{-/-} mice displays mitochondrial dysfunction, ER stress, and inflammation


(37, 38, 76), processes that have been implicated in the development of insulin resistance (37) and reduced cellular glucose uptake (77–80). In line with an alteration in insulin sensitivity, it has been found that, when fed a high-fat diet, *Ucp1*^{-/-} mice display impaired glucose clearance (81). Thus, the lower glucose uptake, as well as the associated reduction of lipogenic enzymes, in BAT of acutely and chronically activated *Ucp1*^{-/-} mice (Figs. 3, 4) may be explained by insulin resistance. On the other hand, in healthy insulin-sensitive BAT of WT mice, glucose uptake reflects thermogenesis. Notably, the lower glucose uptake is also associated with lower thermogenesis known to be present in BAT of UCP1-deficient mice under cold stress (26, 44, 82), which presumably is explained by indirect effects leading to impaired insulin-dependent glucose handling.

Previously, we showed accelerated processing of TRL-derived lipids by activated BAT, and that lipid disposal is dependent on LPL and CD36 expression (11). Consequently, lack of fatty acid transport protein 1 or CD36 impairs thermogenesis when intracellular lipid stores are depleted (11, 83, 84). In line with these results, we found a substantially increased uptake of TRL-derived fatty acids as well as elevated expression of the above-mentioned lipid handling proteins, LPL and CD36, in thermogenic adipose tissues of WT mice after mild and strong activation by cold or CL treatment. Remarkably, this effect was even more pronounced in *Ucp1*^{-/-} mice (Figs. 1, 3, 4), which is probably the result of a higher sympathetic tone in adipose tissues (Figs. 2, 3). The increase leads to higher blood flow into thermogenic adipose tissues and, together with the elevated expression of CD36 and LPL (Figs. 2, 3), explains accelerated TRL processing and uptake of fatty acids in BAT of *Ucp1*^{-/-} mice. The reason for the increased sympathetic tone is currently unknown, but probably results from increased perception of cold in the *Ucp1*^{-/-} mice (85), leading to increased browning of WAT that is also observed in our study (supplemental Fig. S2F, Fig. 3). Another explanation could be increased levels of circulating FGF21 as described for *Ucp1*^{-/-} mice (39). FGF21 has been shown to stimulate WAT browning by altering sympathetic tone (86–88) and promoting lipid disposal into thermogenic adipose tissues (32). The cause of sympathetic tone activation notwithstanding, the question arises whether there is a physiological rationale for the resulting increased lipid uptake in thermogenic adipose tissues. Recently, it has been shown that UCP1-deficient mice use alternative mechanisms for heat production in adipose tissues and other organs. For example, creatine-driven futile cycling in thermogenic adipose tissues of *Ucp1*^{-/-} mice can compensate for the loss of UCP1 (49, 50, 89). In addition, an upregulation of calcium-dependent thermogenesis in adipose tissues and muscle has been suggested. This pathway is thought to involve a sarcolipin-sarco/ER Ca²⁺-ATPase calcium cycling pathway (48, 52, 90–93). In comparison to UCP1-dependent heat production, these mechanisms are probably less efficient and may thus require higher lipid uptake into BAT and WAT to meet their energy demands. Additionally, the increased lipid and glucose uptake into muscles of *Ucp1*^{-/-} mice under these conditions is in line with the sustained

shivering in these mice but may also partially reflect activation of muscle nonshivering thermogenic pathways.

The uptake of lipids in the form of lipoprotein-derived triglycerides accounts for the majority of energy uptake into activated BAT (24). It has, therefore, been proposed that using lipoprotein-embedded fatty acid tracers may greatly improve BAT detection in humans. Such an approach would clearly offer advantages, such as being less susceptible to alterations in insulin sensitivity that might contribute to an underestimation of BAT prevalence in obese diabetic patients when using ^{18}F FDG-PET-CT (23, 94, 95). Our results indicate that lipoprotein tracers might offer the option to detect BAT even in insulin-resistant subjects. However, it has to be kept in mind that based on our studies under UCPI deficiency, lipoprotein handling does not necessarily reflect UCPI-dependent thermogenic activity but rather sympathetic activation of thermogenic adipose tissues.

Data availability

The data supporting this study are available in the article and the supplemental information, and are available from the corresponding author upon reasonable request. 



Acknowledgements

The authors thank Sandra Ehret, Eva Maria Azizi, Birgit Henkel, and Walter Tauscher for excellent technical assistance.

Author contributions

A.W.F., L.S., and J.H. study design; A.W.F., L.S., and J.H. supervision; A.W.F., L.S., and J.H. data analysis; A.W.F., L.S., and J.H. figure preparation; A.W.F., L.S., and J.H. writing; A.W.F., J.B., F.S., C.S., M.H., and P.P. experiments. All authors commented on the manuscript.

Author ORCIDs

Alexander W. Fischer  <https://orcid.org/0000-0001-6717-9090>; Joerg Heeren  <https://orcid.org/0000-0002-5647-1034>

Funding and additional information

This work was supported by Deutsche Forschungsgemeinschaft Grants SCHE522/4 and HE3645/10, the Mühlbauer Stiftung, and the Gertraud und Heinz Rose Stiftung.

Conflict of interest

The authors declare that they have no conflicts of interest with the contents of this article.

Abbreviations

Acaca/ACC, acetyl-CoA carboxylase; Angptl4, angiopoietin-like 4; BAT, brown adipose tissue; CD36, cluster of differentiation 36; CL, CL316,243; CREB, cAMP response element-binding protein; DIO2, deiodinase type 2; Elovl3, elongation of very long chain fatty acids 3; eWAT, epididymal white adipose tissue; GLUT4, glucose transporter 4; g-TUB, γ -tubulin; ^3H -DOG, ^3H -deoxyglucose; HSL, hormone-sensitive lipase; iBAT, interscapular brown adipose tissue; iWAT, inguinal white adipose tissue; OGFT, oral glucose and fat tolerance test; PET-CT, positron emission tomography-computed tomography;

Tbp, TATA-box binding protein; TH, tyrosine hydroxylase; TRL, triglyceride-rich lipoprotein; UCPI, uncoupling protein 1; WAT, white adipose tissue.

Manuscript received October 8, 2019, and in revised form July 9, 2020. Published, JLR Papers in Press, August 7, 2020, DOI 10.1194/jlr.RA119000455.

REFERENCES

1. Cannon, B., and J. Nedergaard. 2004. Brown adipose tissue: function and physiological significance. *Physiol. Rev.* **84**: 277–359.
2. Cypess, A. M., and C. R. Kahn. 2010. The role and importance of brown adipose tissue in energy homeostasis. *Curr. Opin. Pediatr.* **22**: 478–484.
3. Lidell, M. E., M. J. Betz, O. Dahlqvist Leinhard, M. Heglund, L. Elander, M. Slawik, T. Mussack, D. Nilsson, T. Romu, P. Nuutila, et al. 2013. Evidence for two types of brown adipose tissue in humans. *Nat. Med.* **19**: 631–634.
4. Saito, M., Y. Okamatsu-Ogura, M. Matsushita, K. Watanabe, T. Yoneshiro, J. Nio-Kobayashi, T. Iwanaga, M. Miyagawa, T. Kameya, K. Nakada, et al. 2009. High incidence of metabolically active brown adipose tissue in healthy adult humans: effects of cold exposure and adiposity. *Diabetes.* **58**: 1526–1531.
5. Cypess, A. M., S. Lehman, G. Williams, I. Tal, D. Rodman, A. B. Goldfine, F. C. Kuo, E. L. Palmer, Y. H. Tseng, A. Doria, et al. 2009. Identification and importance of brown adipose tissue in adult humans. *N. Engl. J. Med.* **360**: 1509–1517.
6. Virtanen, K. A., M. E. Lidell, J. Orava, M. Heglund, R. Westergren, T. Niemi, M. Taittonen, J. Laine, N. J. Savisto, S. Enerback, et al. 2009. Functional brown adipose tissue in healthy adults. *N. Engl. J. Med.* **360**: 1518–1525.
7. van Marken Lichtenbelt, W. D., J. W. Vanhommerig, N. M. Smulders, J. M. Drossaerts, G. J. Kemerink, N. D. Bouvy, P. Schrauwen, and G. J. Teule. 2009. Cold-activated brown adipose tissue in healthy men. *N. Engl. J. Med.* **360**: 1500–1508.
8. Nedergaard, J., T. Bengtsson, and B. Cannon. 2007. Unexpected evidence for active brown adipose tissue in adult humans. *Am. J. Physiol. Endocrinol. Metab.* **293**: E444–E452.
9. Zingaretti, M. C., F. Crosta, A. Vitali, M. Guerrieri, A. Frontini, B. Cannon, J. Nedergaard, and S. Cinti. 2009. The presence of UCPI1 demonstrates that metabolically active adipose tissue in the neck of adult humans truly represents brown adipose tissue. *FASEB J.* **23**: 3113–3120.
10. Jespersen, N. Z., T. J. Larsen, L. Peijs, S. Dugaard, P. Homoe, A. Loft, J. de Jong, N. Mathur, B. Cannon, J. Nedergaard, et al. 2013. A classical brown adipose tissue mRNA signature partly overlaps with brite in the supraclavicular region of adult humans. *Cell Metab.* **17**: 798–805.
11. Bartelt, A., O. T. Bruns, R. Reimer, H. Hohenberg, H. Itrich, K. Peldschus, M. G. Kaul, U. I. Tromsdorf, H. Weller, C. Waurisch, et al. 2011. Brown adipose tissue activity controls triglyceride clearance. *Nat. Med.* **17**: 200–205.
12. Berbée, J. F., M. R. Boon, P. P. Khedoe, A. Bartelt, C. Schlein, A. Worthmann, S. Kooijman, G. Hoeke, I. M. Mol, C. John, et al. 2015. Brown fat activation reduces hypercholesterolaemia and protects from atherosclerosis development. *Nat. Commun.* **6**: 6356.
13. Stanford, K. L., R. J. Middelbeek, K. L. Townsend, D. An, E. B. Nygaard, K. M. Hitchcox, K. R. Markan, K. Nakano, M. F. Hirshman, Y. H. Tseng, et al. 2013. Brown adipose tissue regulates glucose homeostasis and insulin sensitivity. *J. Clin. Invest.* **123**: 215–223.
14. Bartelt, A., C. John, N. Schaltenberg, J. F. P. Berbee, A. Worthmann, M. L. Cherradi, C. Schlein, J. Piepenburg, M. R. Boon, F. Rinninger, et al. 2017. Thermogenic adipocytes promote HDL turnover and reverse cholesterol transport. *Nat. Commun.* **8**: 15010.
15. Worthmann, A., C. John, M. C. Ruhlemann, M. Baguhl, F. A. Heinsen, N. Schaltenberg, M. Heine, C. Schlein, I. Evangelakos, C. Mineo, et al. 2017. Cold-induced conversion of cholesterol to bile acids in mice shapes the gut microbiome and promotes adaptive thermogenesis. *Nat. Med.* **23**: 839–849.
16. Yoneshiro, T., S. Aita, M. Matsushita, T. Kayahara, T. Kameya, Y. Kawai, T. Iwanaga, and M. Saito. 2013. Recruited brown adipose tissue as an antiobesity agent in humans. *J. Clin. Invest.* **123**: 3404–3408.

17. Matsushita, M., T. Yoneshiro, S. Aita, T. Kameya, H. Sugie, and M. Saito. 2014. Impact of brown adipose tissue on body fatness and glucose metabolism in healthy humans. *Int. J. Obes. (Lond.)*. **38**: 812–817.
18. Lee, P., J. R. Greenfield, K. K. Ho, and M. J. Fulham. 2010. A critical appraisal of the prevalence and metabolic significance of brown adipose tissue in adult humans. *Am. J. Physiol. Endocrinol. Metab.* **299**: E601–E606.
19. Ouellet, V., A. Routhier-Labadie, W. Bellemare, L. Lakhal-Chaieb, E. Turcotte, A. C. Carpentier, and D. Richard. 2011. Outdoor temperature, age, sex, body mass index, and diabetic status determine the prevalence, mass, and glucose-uptake activity of 18F-FDG-detected BAT in humans. *J. Clin. Endocrinol. Metab.* **96**: 192–199.
20. Pfannenberger, C., M. K. Werner, S. Ripkens, I. Stef, A. Deckert, M. Schmadl, M. Reimold, H. U. Haring, C. D. Claussen, and N. Stefan. 2010. Impact of age on the relationships of brown adipose tissue with sex and adiposity in humans. *Diabetes*. **59**: 1789–1793.
21. Blondin, D. P., S. M. Labbe, C. Noll, M. Kunach, S. Phoenix, B. Guerin, E. E. Turcotte, F. Haman, D. Richard, and A. C. Carpentier. 2015. Selective Impairment of Glucose but Not Fatty Acid or Oxidative Metabolism in Brown Adipose Tissue of Subjects With Type 2 Diabetes. *Diabetes*. **64**: 2388–2397.
22. Orava, J., P. Nuutila, T. Noponen, R. Parkkola, T. Viljanen, S. Enerback, A. Rissanen, K. H. Pietilainen, and K. A. Virtanen. 2013. Blunted metabolic responses to cold and insulin stimulation in brown adipose tissue of obese humans. *Obesity (Silver Spring)*. **21**: 2279–2287.
23. Vijgen, G. H., N. D. Bouvy, G. J. Teule, B. Brans, P. Schrauwen, and W. D. van Marken Lichtenbelt. 2011. Brown adipose tissue in morbidly obese subjects. *PLoS One*. **6**: e17247.
24. Heine, M., A. W. Fischer, C. Schlein, C. Jung, L. G. Straub, K. Gottschling, N. Mangels, Y. Yuan, S. K. Nilsson, G. Liebscher, et al. 2018. Lipolysis triggers a systemic insulin response essential for efficient energy replenishment of activated brown adipose tissue in mice. *Cell Metab.* **28**: 644–655.e4.
25. Hankir, M. K., and M. Klingenspor. 2018. Brown adipocyte glucose metabolism: a heated subject. *EMBO Rep.* **19**: e46404.
26. Enerbäck, S., A. Jacobsson, E. M. Simpson, C. Guerra, H. Yamashita, M. E. Harper, and L. P. Kozak. 1997. Mice lacking mitochondrial uncoupling protein are cold-sensitive but not obese. *Nature*. **387**: 90–94.
27. Feldmann, H. M., V. Golozoubova, B. Cannon, and J. Nedergaard. 2009. UCPI ablation induces obesity and abolishes diet-induced thermogenesis in mice exempt from thermal stress by living at thermoneutrality. *Cell Metab.* **9**: 203–209.
28. Luijten, I. H. N., H. M. Feldmann, G. von Essen, B. Cannon, and J. Nedergaard. 2019. In the absence of UCPI-mediated diet-induced thermogenesis, obesity is augmented even in the obesity-resistant 129S mouse strain. *Am. J. Physiol. Endocrinol. Metab.* **316**: E729–E740.
29. Fischer, A. W., B. Cannon, and J. Nedergaard. 2018. Optimal housing temperatures for mice to mimic the thermal environment of humans: An experimental study. *Mol. Metab.* **7**: 161–170.
30. Fischer, A. W., B. Cannon, and J. Nedergaard. 2019. The answer to the question “What is the best housing temperature to translate mouse experiments to humans?” is: thermoneutrality. *Mol. Metab.* **26**: 1–3.
31. de Jong, J. M. A., W. Sun, N. D. Pires, A. Frontini, M. Balaz, K. Petrovic, A. W. Fischer, M. H. Bokhari, T. Niemi, P. Nuutila, et al. 2019. Human brown adipose tissue is phenocopied by classical brown (but not beige) adipose tissue in physiologically humanized mice. *Nat. Metab.* **1**: 830–843.
32. Schlein, C., S. Talukdar, M. Heine, A. W. Fischer, L. M. Krott, S. K. Nilsson, M. B. Brenner, J. Heeren, and L. Scheja. 2016. FGF21 lowers plasma triglycerides by accelerating lipoprotein catabolism in white and brown adipose tissues. *Cell Metab.* **23**: 441–453.
33. Fischer, A. W., K. Albers, L. M. Krott, B. Hoffzimmer, M. Heine, H. Schmale, L. Scheja, P. Gordts, and J. Heeren. 2018. The adaptor protein PID1 regulates receptor-dependent endocytosis of post-prandial triglyceride-rich lipoproteins. *Mol. Metab.* **16**: 88–99.
34. Fischer, A. W., K. Albers, C. Schlein, F. Sass, L. M. Krott, H. Schmale, P. L. S. M. Gordts, L. Scheja, and J. Heeren. 2019. PID1 regulates insulin-dependent glucose uptake by controlling intracellular sorting of GLUT4-storage vesicles. *Biochim. Biophys. Acta Mol. Basis Dis.* **1865**: 1592–1603.
35. Fischer, A. W., C. Schlein, B. Cannon, J. Heeren, and J. Nedergaard. 2019. Intact innervation is essential for diet-induced recruitment of brown adipose tissue. *Am. J. Physiol. Endocrinol. Metab.* **316**: E487–E503.
36. Galarraga, M., J. Campión, A. Muñoz-Barrutia, N. Boqué, H. Moreno, J. A. Martínez, F. Milagro, and C. Ortiz-de-Solórzano. 2012. Adiposoft: automated software for the analysis of white adipose tissue cellularity in histological sections. *J. Lipid Res.* **53**: 2791–2796.
37. Keipert, S., M. Kutschke, M. Ost, T. Schwarzmayr, E. M. van Schothorst, D. Lamp, L. Brachthäuser, I. Hamp, S. E. Mazibuko, S. Hartwig, et al. 2017. Long-term cold adaptation does not require FGF21 or UCPI. *Cell Metab.* **26**: 437–446.e5.
38. Bond, L. M., M. S. Burhans, and J. M. Ntambi. 2018. Uncoupling protein-1 deficiency promotes brown adipose tissue inflammation and ER stress. *PLoS One*. **13**: e0205726.
39. Keipert, S., M. Kutschke, D. Lamp, L. Brachthäuser, F. Neff, C. W. Meyer, R. Oelkrug, A. Kharitonov, and M. Jastroch. 2015. Genetic disruption of uncoupling protein 1 in mice renders brown adipose tissue a significant source of FGF21 secretion. *Mol. Metab.* **4**: 537–542.
40. Bond, L. M., and J. M. Ntambi. 2018. UCPI deficiency increases adipose tissue monounsaturated fatty acid synthesis and trafficking to the liver. *J. Lipid Res.* **59**: 224–236.
41. Sanchez-Gurmaches, J., Y. Tang, N. Z. Jespersen, M. Wallace, C. Martinez Calejman, S. Gujja, H. Li, Y. J. K. Edwards, C. Wolfrum, C. M. Metallo, et al. 2018. Brown fat AKT2 is a cold-induced kinase that stimulates ChREBP-mediated de novo lipogenesis to optimize fuel storage and thermogenesis. *Cell Metab.* **27**: 195–209.e6.
42. Dijk, W., M. Heine, L. Vergnes, M. R. Boon, G. Schaart, M. K. Hesselink, K. Reue, W. D. van Marken Lichtenbelt, G. Olivecrona, P. C. Rensen, et al. 2015. ANGPTL4 mediates shuttling of lipid fuel to brown adipose tissue during sustained cold exposure. *eLife*. **4**: e08428.
43. Lynes, M. D., L. O. Leiria, M. Lundh, A. Bartelt, F. Shamsi, T. L. Huang, H. Takahashi, M. F. Hirshman, C. Schlein, A. Lee, et al. 2017. The cold-induced lipokine 12,13-diHOME promotes fatty acid transport into brown adipose tissue. *Nat. Med.* **23**: 631–637.
44. Golozoubova, V., E. Hohtola, A. Matthias, A. Jacobsson, B. Cannon, and J. Nedergaard. 2001. Only UCPI can mediate adaptive nonshivering thermogenesis in the cold. *FASEB J.* **15**: 2048–2050.
45. Shabalina, I. G., J. Hoeks, T. V. Kramarova, P. Schrauwen, B. Cannon, and J. Nedergaard. 2010. Cold tolerance of UCPI-ablated mice: a skeletal muscle mitochondria switch toward lipid oxidation with marked UCP3 up-regulation not associated with increased basal, fatty acid- or ROS-induced uncoupling or enhanced GDP effects. *Biochim. Biophys. Acta*. **1797**: 968–980.
46. Shabalina, I. G., N. Petrovic, J. M. de Jong, A. V. Kalinovich, B. Cannon, and J. Nedergaard. 2013. UCPI in brite/beige adipose tissue mitochondria is functionally thermogenic. *Cell Rep.* **5**: 1196–1203.
47. Golozoubova, V., B. Cannon, and J. Nedergaard. 2006. UCPI is essential for adaptive adrenergic nonshivering thermogenesis. *Am. J. Physiol. Endocrinol. Metab.* **291**: E350–E357.
48. Ukropec, J., R. P. Anunciado, Y. Ravussin, M. W. Hulver, and L. P. Kozak. 2006. UCPI-independent thermogenesis in white adipose tissue of cold-acclimated Ucp1^{-/-} mice. *J. Biol. Chem.* **281**: 31894–31908.
49. Kazak, L., E. T. Chouchani, M. P. Jedrychowski, B. K. Erickson, K. Shinoda, P. Cohen, R. Vetrivelan, G. Z. Lu, D. Laznik-Bogoslavski, S. C. Hasenfuss, et al. 2015. A creatine-driven substrate cycle enhances energy expenditure and thermogenesis in beige fat. *Cell*. **163**: 643–655.
50. Kazak, L., E. T. Chouchani, G. Z. Lu, M. P. Jedrychowski, C. J. Bare, A. I. Mina, M. Kumari, S. Zhang, I. Vuckovic, D. Laznik-Bogoslavski, et al. 2017. Genetic depletion of adipocyte creatine metabolism inhibits diet-induced thermogenesis and drives obesity. *Cell Metab.* **26**: 693.
51. Chouchani, E. T., L. Kazak, and B. M. Spiegelman. 2019. New advances in adaptive thermogenesis: UCPI and beyond. *Cell Metab.* **29**: 27–37.
52. Bal, N. C., S. K. Maurya, D. H. Sopariwala, S. K. Sahoo, S. C. Gupta, S. A. Shaikh, M. Pant, L. A. Rowland, E. Bombardier, S. A. Goonasekera, et al. 2012. Sarcosine is a newly identified regulator of muscle-based thermogenesis in mammals. *Nat. Med.* **18**: 1575–1579. [Erratum. 2012. *Nat. Med.* **18**: 1857.]
53. Wu, J., P. Bostrom, L. M. Sparks, L. Ye, J. H. Choi, A. H. Giang, M. Khandekar, K. A. Virtanen, P. Nuutila, G. Schaart, et al. 2012. Beige adipocytes are a distinct type of thermogenic fat cell in mouse and human. *Cell*. **150**: 366–376.
54. Petrovic, N., I. G. Shabalina, J. A. Timmons, B. Cannon, and J. Nedergaard. 2008. Thermogenically competent nonadrenergic recruitment in brown preadipocytes by a PPARgamma agonist. *Am. J. Physiol. Endocrinol. Metab.* **295**: E287–E296.

55. Bartelt, A., and J. Heeren. 2014. Adipose tissue browning and metabolic health. *Nat. Rev. Endocrinol.* **10**: 24–36.
56. Randle, P. J., P. B. Garland, C. N. Hales, and E. A. Newsholme. 1963. The glucose fatty-acid cycle. Its role in insulin sensitivity and the metabolic disturbances of diabetes mellitus. *Lancet.* **1**: 785–789.
57. Olsen, J. M., R. I. Csikasz, N. Dehvari, L. Lu, A. Sandstrom, A. I. Oberg, J. Nedergaard, S. Stone-Elander, and T. Bengtsson. 2017. beta3-Adrenergically induced glucose uptake in brown adipose tissue is independent of UCP1 presence or activity: mediation through the mTOR pathway. *Mol. Metab.* **6**: 611–619.
58. Inokuma, K., Y. Ogura-Okamatsu, C. Toda, K. Kimura, H. Yamashita, and M. Saito. 2005. Uncoupling protein 1 is necessary for norepinephrine-induced glucose utilization in brown adipose tissue. *Diabetes.* **54**: 1385–1391.
59. Furler, S. M., G. J. Cooney, B. D. Hegarty, M. Y. Lim-Fraser, E. W. Kraegen, and N. D. Oakes. 2000. Local factors modulate tissue-specific NEFA utilization: assessment in rats using 3H-(R)-2-bromopalmitate. *Diabetes.* **49**: 1427–1433.
60. Henkin, A. H., A. S. Cohen, E. A. Dubikovskaya, H. M. Park, G. F. Nikitin, M. G. Auzias, M. Kazantzis, C. R. Bertozzi, and A. Stahl. 2012. Real-time noninvasive imaging of fatty acid uptake in vivo. *ACS Chem. Biol.* **7**: 1884–1891.
61. Liu, X., F. Perusse, and L. J. Bukowiecki. 1994. Chronic norepinephrine infusion stimulates glucose uptake in white and brown adipose tissues. *Am. J. Physiol.* **266**: R914–R920.
62. Ma, S. W., and D. O. Foster. 1986. Uptake of glucose and release of fatty acids and glycerol by rat brown adipose tissue in vivo. *Can. J. Physiol. Pharmacol.* **64**: 609–614.
63. Orava, J., P. Nuutila, M. E. Lidell, V. Oikonen, T. Noponen, T. Viljanen, M. Scheinin, M. Taittonen, T. Niemi, S. Enerback, et al. 2011. Different metabolic responses of human brown adipose tissue to activation by cold and insulin. *Cell Metab.* **14**: 272–279.
64. Cypess, A. M., L. S. Weiner, C. Roberts-Toler, E. Franquet Elia, S. H. Kessler, P. A. Kahn, J. English, K. Chatman, S. A. Trauger, A. Doria, et al. 2015. Activation of human brown adipose tissue by a beta3-adrenergic receptor agonist. *Cell Metab.* **21**: 33–38.
65. Ouellet, V., S. M. Labbe, D. P. Blondin, S. Phoenix, B. Guerin, F. Haman, E. E. Turcotte, D. Richard, and A. C. Carpentier. 2012. Brown adipose tissue oxidative metabolism contributes to energy expenditure during acute cold exposure in humans. *J. Clin. Invest.* **122**: 545–552.
66. Blondin, D. P., H. C. Tingelstad, C. Noll, F. Frisch, S. Phoenix, B. Guerin, E. E. Turcotte, D. Richard, F. Haman, and A. C. Carpentier. 2017. Dietary fatty acid metabolism of brown adipose tissue in cold-acclimated men. *Nat. Commun.* **8**: 14146.
67. Paulus, A., N. Drude, E. B. M. Nascimento, E. M. Buhl, J. F. P. Berbee, P. C. N. Rensen, W. D. van Marken Lichtenbelt, F. M. Mottaghy, and M. Bauwens. 2019. [(18)F]BODIPY-triglyceride-containing chylomicron-like particles as an imaging agent for brown adipose tissue in vivo. *Sci. Rep.* **9**: 2706.
68. Hankir, M. K., M. Kranz, S. Keipert, J. Weiner, S. G. Andreasen, M. Kern, M. Patt, N. Kloting, J. T. Heiker, P. Brust, et al. 2017. Dissociation between brown adipose tissue (18)F-FDG uptake and thermogenesis in uncoupling protein 1-deficient mice. *J. Nucl. Med.* **58**: 1100–1103.
69. Jeanguillaume, C., G. Metrard, D. Ricquier, P. Legras, F. Bouchet, F. Lacoeuille, F. Hindre, O. Morel, and H. Rakotonirina. 2013. Visualization of activated BAT in mice, with FDG-PET and its relation to UCP1. *Adv. J. Mol. Imaging.* **3**: 19–22.
70. Olsen, J. M., M. Sato, O. S. Dallner, A. L. Sandstrom, D. F. Pisani, J. C. Chambard, E. Z. Amri, D. S. Hutchinson, and T. Bengtsson. 2014. Glucose uptake in brown fat cells is dependent on mTOR complex 2-promoted GLUT1 translocation. *J. Cell Biol.* **207**: 365–374.
71. Winther, S., M. S. Isidor, A. L. Basse, N. Skjoldborg, A. Cheung, B. Quistorff, and J. B. Hansen. 2018. Restricting glycolysis impairs brown adipocyte glucose and oxygen consumption. *Am. J. Physiol. Endocrinol. Metab.* **314**: E214–E223.
72. Isler, D., H. P. Hill, and M. K. Meier. 1987. Glucose metabolism in isolated brown adipocytes under beta-adrenergic stimulation. Quantitative contribution of glucose to total thermogenesis. *Biochem. J.* **245**: 789–793.
73. Irshad, Z., F. Dimitri, M. Christian, and V. A. Zammit. 2017. Diacylglycerol acyltransferase 2 links glucose utilization to fatty acid oxidation in the brown adipocytes. *J. Lipid Res.* **58**: 15–30.
74. Yu, X. X., D. A. Lewin, W. Forrest, and S. H. Adams. 2002. Cold elicits the simultaneous induction of fatty acid synthesis and beta-oxidation in murine brown adipose tissue: prediction from differential gene expression and confirmation in vivo. *FASEB J.* **16**: 155–168.
75. Scheja, L., L. Makowski, K. T. Uysal, S. M. Wiesbrock, D. R. Shimshek, D. S. Meyers, M. Morgan, R. A. Parker, and G. S. Hotamisligil. 1999. Altered insulin secretion associated with reduced lipolytic efficiency in aP2-/- mice. *Diabetes.* **48**: 1987–1994.
76. Kazak, L., E. T. Chouchani, I. G. Stavrovskaya, G. Z. Lu, M. P. Jedrychowski, D. F. Egan, M. Kumari, X. Kong, B. K. Erickson, J. Szpyt, et al. 2017. UCP1 deficiency causes brown fat respiratory chain depletion and sensitizes mitochondria to calcium overload-induced dysfunction. *Proc. Natl. Acad. Sci. USA.* **114**: 7981–7986.
77. Kammoun, H. L., M. J. Kraakman, and M. A. Febbraio. 2014. Adipose tissue inflammation in glucose metabolism. *Rev. Endocr. Metab. Disord.* **15**: 31–44.
78. Shah, A., N. Mehta, and M. P. Reilly. 2008. Adipose inflammation, insulin resistance, and cardiovascular disease. *JPEN J. Parenter. Enteral Nutr.* **32**: 638–644.
79. Wang, X., C. O. Eno, B. J. Altman, Y. Zhu, G. Zhao, K. E. Olberding, J. C. Rathmell, and C. Li. 2011. ER stress modulates cellular metabolism. *Biochem. J.* **435**: 285–296.
80. van der Harg, J. M., J. C. van Heest, F. N. Bangel, S. Patiwaal, J. R. T. van Weering, and W. Scheper. 2017. The UPR reduces glucose metabolism via IRE1 signaling. *Biochim. Biophys. Acta Mol. Cell Res.* **1864**: 655–665.
81. Maurer, S. F., T. Fromme, S. Mocek, A. Zimmermann, and M. Klingenspor. 2020. Uncoupling protein 1 and the capacity for non-shivering thermogenesis are components of the glucose homeostatic system. *Am. J. Physiol. Endocrinol. Metab.* **318**: E198–E215.
82. Nedergaard, J., V. Golozoubova, A. Matthias, I. Shabalina, K. Ohba, K. Ohlson, A. Jacobsson, and B. Cannon. 2001. Life without UCP1: mitochondrial, cellular and organismal characteristics of the UCP1-ablated mice. *Biochem. Soc. Trans.* **29**: 756–763.
83. Putri, M., M. R. Syamsunarno, T. Iso, A. Yamaguchi, H. Hanaoka, H. Sunaga, N. Koitabashi, H. Matsui, C. Yamazaki, S. Kameo, et al. 2015. CD36 is indispensable for thermogenesis under conditions of fasting and cold stress. *Biochem. Biophys. Res. Commun.* **457**: 520–525.
84. Wu, Q., M. Kazantzis, H. Doerge, A. M. Ortegon, B. Tsang, A. Falcon, and A. Stahl. 2006. Fatty acid transport protein 1 is required for nonshivering thermogenesis in brown adipose tissue. *Diabetes.* **55**: 3229–3237.
85. Nedergaard, J., and B. Cannon. 2014. The browning of white adipose tissue: some burning issues. *Cell Metab.* **20**: 396–407.
86. Fisher, F. M., S. Kleiner, N. Douris, E. C. Fox, R. J. Mepani, F. Verdeguer, J. Wu, A. Kharitonov, J. S. Flier, E. Maratos-Flier, et al. 2012. FGF21 regulates PGC-1alpha and browning of white adipose tissues in adaptive thermogenesis. *Genes Dev.* **26**: 271–281.
87. Owen, B. M., X. Ding, D. A. Morgan, K. C. Coate, A. L. Bookout, K. Rahmouni, S. A. Klierer, and D. J. Mangelsdorf. 2014. FGF21 acts centrally to induce sympathetic nerve activity, energy expenditure, and weight loss. *Cell Metab.* **20**: 670–677.
88. Douris, N., D. M. Stevanovic, F. M. Fisher, T. I. Cisu, M. J. Chee, N. L. Nguyen, E. Zarebidaki, A. C. Adams, A. Kharitonov, J. S. Flier, et al. 2015. Central fibroblast growth factor 21 browns white fat via sympathetic action in male mice. *Endocrinology.* **156**: 2470–2481.
89. Reilly, S. M., and A. R. Saltiel. 2015. A futile approach to fighting obesity? *Cell.* **163**: 539–540.
90. Ukropec, J., R. V. Anunciado, Y. Ravussin, and L. P. Kozak. 2006. Leptin is required for uncoupling protein-1-independent thermogenesis during cold stress. *Endocrinology.* **147**: 2468–2480.
91. Rowland, L. A., S. K. Maurya, N. C. Bal, L. Kozak, and M. Periasamy. 2016. Sarcosine and uncoupling protein 1 play distinct roles in diet-induced thermogenesis and do not compensate for one another. *Obesity (Silver Spring).* **24**: 1430–1433.
92. Bal, N. C., S. K. Maurya, S. Singh, X. H. T. Wehrens, and M. Periasamy. 2016. Increased reliance on muscle-based thermogenesis upon acute minimization of brown adipose tissue function. *J. Biol. Chem.* **291**: 17247–17257.
93. Ikeda, K., Q. Kang, T. Yoneshiro, J. P. Camporez, H. Maki, M. Homma, K. Shinoda, Y. Chen, X. Lu, P. Maretich, et al. 2017. UCP1-independent signaling involving SERCA2b-mediated calcium cycling regulates beige fat thermogenesis and systemic glucose homeostasis. *Nat. Med.* **23**: 1454–1465.
94. Paulus, A., W. van Marken Lichtenbelt, F. M. Mottaghy, and M. Bauwens. 2017. Brown adipose tissue and lipid metabolism imaging. *Methods.* **130**: 105–113.
95. Moonen, M. P. B., E. B. M. Nascimento, and W. D. van Marken Lichtenbelt. 2019. Human brown adipose tissue: Underestimated target in metabolic disease? *Biochim. Biophys. Acta Mol. Cell Biol. Lipids.* **1864**: 104–112.